Open Archive TOULOUSE Archive Ouverte (OATAO)

OATAO is an open access repository that collects the work of Toulouse researchers and makes it freely available over the web where possible.

This is an author-deposited version published in : http://oatao.univ-toulouse.fr/
Eprints ID : 15135

To link to this article : DOI : 10.1002/pssa.201532838
URL : http://dx.doi.org/10.1002/pssa.201532838

To cite this version : Baggetto, Loïc and Charvillat, Cédric and Thebault, Yannick and Esvan, Jérôme and Lafont, Marie-Christine and Scheid, Emmanuel and Veith, Gabriel M. and Vahlas, Constantin *Amorphous alumina thin films deposited on titanium:*

Any correspondance concerning this service should be sent to the repository administrator: staff-oatao@listes-diff.inp-toulouse.fr

Amorphous alumina thin films deposited on titanium: Interfacial chemistry and thermal oxidation barrier properties

Loïc Baggetto[*,1], Cédric Charvillat[1], Yannick Thébault[1], Jérôme Esvan[1], Marie-Christine Lafont[1], Emmanuel Scheid[2], Gabriel M. Veith[3], and Constantin Vahlas[,1]**

[1] Centre Inter-universitaire de Recherche et d'Ingéniérie des Matériaux (CIRIMAT), UMR5085 CNRS, 4 allée Emile Monso, BP-44362, 31030 Toulouse Cedex 4, France

[2] Laboratoire d'Analyse et d'Architecture des Systèmes (LAAS), CNRS, 7 Avenue du colonel Roche, 31400 Toulouse, France

[3] Materials Science and Technology Division, Oak Ridge National Laboratory, 1 Bethel Valley Road, Oak Ridge 37831, TN, USA

Keywords deposition, interdiffusion, oxygen barriers, thin films, Ti/Al_2O_3, X-ray photoelectron spectroscopy

* Corresponding author: e-mail loic_baggetto@yahoo.fr, Phone: +33534323430, Fax: +33534323498

** e-mail constantin.vahlas@ensiacet.fr

Ti/Al_2O_3 bilayer stacks are used as model systems to investigate the role of atomic layer deposition (ALD) and chemical vapor deposition (CVD) to prepare 30–180 nm thick amorphous alumina films as protective barriers for the medium temperature oxidation (500–600 °C) of titanium, which is employed in aeronautic applications. X-ray diffraction (XRD), transmission electron microscopy (TEM) with selected area electron diffraction (SAED), and X-ray photoelectron spectroscopy (XPS) results show that the films produced from the direct liquid injection (DLI) CVD of aluminum tri-isopropoxide (ATI) are poor oxygen barriers. The films processed using the ALD of trimethylaluminum (TMA) show good barrier properties but an extensive intermixing with Ti which subsequently oxidizes. In contrast, the films prepared from dimethyl aluminum isopropoxide (DMAI) by CVD are excellent oxygen barriers and show little intermixing with Ti. Overall, these measurements correlate the effect of the alumina coating thickness, morphology, and stoichiometry resulting from the preparation method to the oxidation barrier properties, and show that compact and stoichiometric amorphous alumina films offer superior barrier properties.

1 Introduction Nowadays, aluminum oxide, commonly referred to as alumina, is a key component of various products, devices, and equipment. For instance, alumina is extensively employed as a dielectric material in capacitors and other electrical devices, as substrate and furnace materials, filler in cosmetic formulations, hard coatings and soft abrasives, and as support for catalysis [1–5]. The widespread use of alumina is intimately linked to the functional properties of its various crystallographic polymorphs (corundum, sapphire, gamma alumina, etc.) [6]. Recently, there has been a surge of interest for the use of alumina films as a protective barrier for lithium-ion battery electrode materials as alumina films prepared by atomic layer deposition (ALD) and magnetron sputtering can significantly reduce electrolyte side reactions and increase the battery lifetime of future electric cars [7–9]. Alumina produced by ALD has also shown great promises as passivation layer of TiO_2 in organic solar cells [10]. Apart from these applications, it is well known that alumina can be used as a barrier material for corrosion and medium temperature (400–600 °C) oxidation to serve as a protection for metallic alloys used for instance in the aeronautics [11, 12].

The use of thermal and oxygen barriers is critical for aeronautic applications where engine parts can be exposed to temperatures from few hundred to more than a thousand degrees Celsius, with a steady push to increase the turbofan engine temperature in order to increase fuel combustion efficiency [13, 14]. Titanium alloys are widely used

materials in the cooler part of the engine where the temperature does not exceed 600 °C [15]. The chemical reactivity between alumina and titanium was formerly studied using powder and thin film model systems with emphasis on intermetallic and ternary compound formation [16–19]. However, the works did not focus on the relationships between the oxidation of Ti and the morphology, thickness, and composition of the films resulting from the processing conditions.

In the present article, we investigate the interaction between titanium, the base material used in the medium temperature engine parts, and three types of amorphous alumina thin films prepared by ALD and chemical vapor deposition (CVD) as protection barriers against thermal oxidation. ALD and CVD are powerful techniques to uniformly cover topologically complex objects or substrates [20–22], as demonstrated by the widespread use of the preparation methods in the microelectronic and glass coating industries [23–25]. Moreover, these preparation techniques can be controlled to yield amorphous alumina films that have optimal oxygen barrier and mechanical properties, as shown for CVD films obtained from evaporated aluminum tri-isopropoxide (ATI) precursor [26–28]. Herein, we will discuss the properties of Ti/Al_2O_3 bilayer model systems with emphasis on the structure, interfacial chemistry, and oxygen barrier properties before and after annealing at 500 and 600 °C in air as function of Al_2O_3 process. Results on bilayer stacks prepared from sputtered titanium and alumina films processed using the DLI CVD of ATI, named DLI ATI hereafter, and DLI CVD of dimethyl aluminum isopropoxide (DMAI), named DLI DMAI hereafter, will be discussed. We have used these CVD precursors as they can deliver amorphous alumina films at moderate temperatures, are relatively cheap, safe, and easy to handle [29, 30]. These results are contrasted to ALD grown Al_2O_3 from trimethyl aluminum (TMA) precursor on the same Ti base layer. For studying the surface and bulk properties, such as phase formation and intermixing, we have employed atomic force microscopy (AFM), X-ray diffraction (XRD), high resolution transmission electron microscopy (HRTEM) coupled with selective area electron diffraction (SAED), and X-ray photoelectron spectroscopy (XPS) combined with Ar ion etching. Special attention is given to the relationship between the physico-chemical properties of alumina (composition, thickness, and morphology) and the barrier performance measured by the extent of titanium oxidation and the interdiffusion between titanium and alumina.

2 Experimental

2.1 Thin film preparation Ti thin films were prepared by DC magnetron sputtering in a custom-built reactor pumped down to a base pressure of 5.10^{-7} Torr or less. Pre-sputtering was conducted for 20 min on a polycrystalline Ti target (99.97%, Lesker) using an Ar (99.9995%, Air Liquide) plasma at 40 W power and 5 mTorr deposition pressure, and a target-substrate distance of 5 cm. Deposition took place onto polished Si (001) wafers (University wafer). Thickness was calibrated using a quartz microbalance mounted inside the chamber. Under the present conditions, the growth rate was measured to be about 34 nm min^{-1} and four nominal thicknesses from 100 to 1000 nm were prepared. After deposition, the Si wafers covered with Ti films were cut into small squares of 5×5 or 7×7 mm^2 for alumina deposition.

Al_2O_3 amorphous thin films were prepared onto samples of Si covered with Ti films and Si blank samples (Sil'tronix). ALD was performed in a Fiji apparatus (Nanothech). ALD cycles with TMA and an oxygen remote plasma (300 W) as reactants were employed. Deposition was carried out at substrate temperature of 300 °C and working pressure of about 70 mTorr. Each cycle consisted of 15 ms TMA dosing time, 5 s TMA purge, 20 sccm O_2 dosing during 5 s stabilization followed by plasma exposure for 20 s, and a final purge of 5 s.

DLI CVD was performed in a homemade horizontal hot-wall reactor equipped with four gas lines and mass flow controllers (MFC), a large evaporation stainless steel chamber and a quartz tube (25 mm diameter, 300 mm length) heated by a resistive furnace described previously [29, 30]. In short, samples were placed on a stainless steel holder in the center of the quartz tube where the temperature was uniform, with a total reaction pressure of 5 Torr. Gas lines and the evaporation steel chamber were heated to *ca.* 80 or 130 °C to prevent DMAI or ATI vapor condensation, respectively. ATI powder (>98%, Acros Organics) or DMAI liquid (>99%, Air Liquide) precursors were weighted and sealed inside a Schlenk flask inside a glovebox circulated with purified Ar (99.9997%, Air Products). The sealed flask was taken out of the glovebox and filled with the appropriate quantity of anhydrous cyclohexane (99.5%, $H_2O < 10$ ppm, Sigma–Aldrich) using an air-tight, Ar-purged, glass syringe to prepare solutions of 0.2 M. Then, the Schlenk flask was connected to the injection system and purged several times with pressurized N_2 (99.9999%, Praxair). The frequency and opening times of the injection system (Kemstream) were controlled to feed the evaporation chamber with precursor solution microdroplets mixed with N_2 gas having a flow set from 300 to 400 sccm. For DMAI precursor, 50 sccm O_2 was added to the dilution gas. Deposition was generally carried out at 420 and 500 °C for ATI and DMAI precursors, respectively. For ATI precursor, some deposition runs were also conducted at 485 °C. Process conditions are summarized in Table 1.

Films were post-annealed at 500 and 600 °C for 65 h in a horizontal tube furnace kept in air. Heating was operated at 60 °C min^{-1} followed by a plateau of 65 h followed by natural cooling to room temperature after which the samples were carefully removed from the oven for further characterization.

2.2 Materials characterization The film thickness was measured on Si witness samples using optical

Table 1 Process parameters used during the preparation of alumina thin films. Cyclohexane solvent, a total pressure of 5 Torr, and opening frequency and injection times of 2 Hz and 5 ms were used for the DLI CVD processes. Growth rate is in nm h^{-1} and nm $cycle^{-1}$ for the DLI CVD and ALD processes, respectively.

temperature (°C)	process	precursor	gas	injection mixing flow (sccm)	dilution flow (sccm)	growth rate (nm h^{-1} or nm $cycle^{-1}$)
500	DLI CVD	DMAI	N_2/O_2	400	400	300
420	DLI CVD	ATI	N_2	300	300	1400
300	ALD	TMA	O_2	n/a	n/a	0.09

reflectivity (Mikropack, Nanocalc 2000). Samples surface morphology and roughness were measured using AFM in ambient conditions on an Agilent Technologies 5500. Scanning was performed in contact mode with tips of spring constant of about 0.292 N m^{-1} (AppNano). Scanning rate was set to 2 μm s^{-1}. The film crystalline structure was measured by XRD on a Bruker D8 Advance using a Cu K_α (1.5418 Å) X-ray tube operated at 40 kV and 40 mA, a Ni filter and solid-state Lynxeye detector in $\theta + 3°/\theta - 3°$ configuration. Samples were measured on a zero background holder and a θ offset of 3° was applied between the source and detector arms to suppress the strong (004) diffraction of the Si substrate normally measured around 68–69°. SEM micrographs were taken in backscattered mode on a JEOL JSM-7800F field emission SEM operated at 10 kV. SEM samples were fractured then covered by a thin layer of sputtered platinum to prevent charging effects.

For TEM observations, cross-sections of the CVD deposit were prepared by cutting the substrates into thin slices with a diamond wire saw. Two slices were glued face to face and embedded in a 3 mm diameter brass tube with epoxy resin. After curing, the tube was sectioned into approximately 300 μm thick discs. These discs were then mechanically polished on both faces with a tripod polisher and diamond clothes down to 100 μm and finally dimpled with a South Bay Technology Dimpler before ion-milling to achieve electron transparency, with a low angle (0–10°) GATAN precision ion-beam polishing system. TEM coupled with SAED was measured using a JEOL JEM 2100F microscope operated at 200 kV and equipped with a Bruker energy dispersive X-ray spectrometer (EDX) for chemical analysis.

XPS measurements were performed on a Thermo Scientific K-Alpha instrument capable of a typical base pressure of 10^{-9} Torr using monochromatic Al K_α (1486.7 eV). The spectrometer energy calibration was performed using the Au $4f_{7/2}$ (83.9 ± 0.1 eV) and Cu $2p_{3/2}$ (932.7 ± 0.1 eV) photoelectron lines. Charging compensation and neutralization were applied by using a dual beam flood gun. The probed areas were about 400 μm diameter. Constant pass energy of 30 eV and energy steps of 0.1 eV were used for high-resolution scans. Surface erosion was employed using Ar ions accelerated at 2 keV, resulting for alumina in an erosion rate of about 0.08 nm s^{-1}. The atomic concentrations were determined from photoelectron peak areas using the atomic sensitivity factors reported by Scofield, taking into account the transmission function of the analyzer. This function was calculated at different pass energies from Ag3d and AgMNN peaks collected for a silver reference sample.

3 Results and discussion The surface morphology and roughness measured by AFM of 100 nm thick Ti films before and after deposition of amorphous alumina are shown in Fig. 1, and the corresponding roughness parameters are listed in Table 2. The surface of the pristine Ti films presents a needle-like morphology with an arithmetic roughness S_a of 5.1 nm and a root mean squared roughness value S_q of 6.3 nm over an area of 4 μm^2. During the growth of alumina films onto polished Si substrates, the nuclei density and surface diffusion of precursors are high enough to produce very smooth films (see Supporting Information (in the following named as SI), Fig. S1, online at www.pss-a.com) with roughness parameters S_a and S_q of 0.6 and 0.8 nm for the DLI DMAI films, of 1.9 and 2.4 nm for the DLI ATI films, and of 0.2 and 0.3 nm for the ALD films (Table 2). When alumina deposition takes place onto the surface of Ti films, the bilayer stack surfaces are generally accompanied with a decrease of the roughness with regard to the Ti starting surface. The ALD films, which are extremely smooth when deposited onto Si, yield smoother surfaces whereas the CVD films, which are somewhat less smooth than the ALD films, lead to the formation of rougher surfaces when deposited onto Ti. Indeed, the ALD of alumina leads to the formation of peaks with larger lateral widths and lower heights, resulting in a lower surface roughness, in particular for the thicker film of 70 nm with S_a and S_q values of about 3.0 and 3.8 nm, respectively. For the films prepared by CVD, the morphology resembles more closely that of the starting Ti surface, in particular for the DLI ATI film, accompanied with higher roughness parameters of about 4.5 for S_a and 5.6 nm for S_q.

The morphology of the films was further investigated using SEM on cross-sections prepared for Si/Al_2O_3 (SI Fig. S2) and $Si/Ti/Al_2O_3$ (Fig. 2 and SI Fig. S2) systems. Similar surface morphologies and roughness were observed in the SEM photographs and surface AFM measurements. Cross-sections photographs better reveal the internal structure of the films. Alumina films prepared onto Ti by ALD and DLI DMAI have a compact structure (Fig. 2a, b, and d), which is similar to that obtained for alumina films

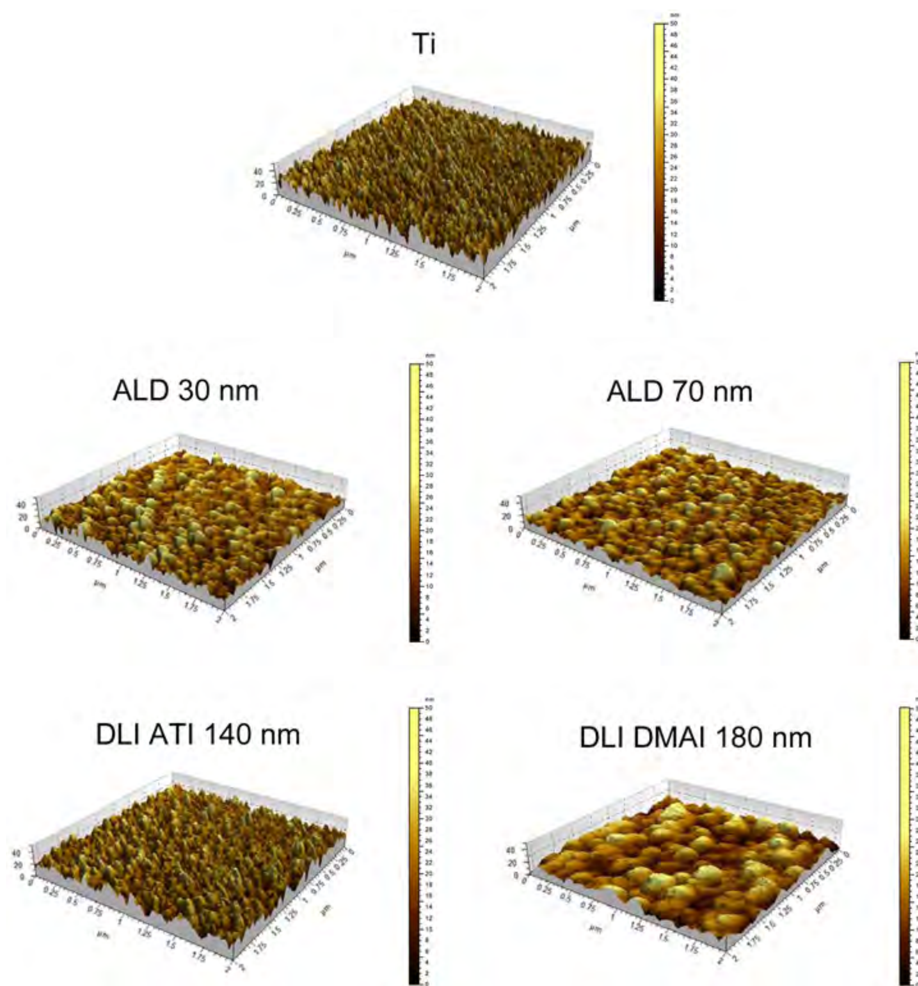

Figure 1 3D topography images of alumina surfaces measured by contact AFM for 100 nm thick Ti and 100 nm thick Ti films covered by 30 nm of ALD Al_2O_3, 70 nm of ALD Al_2O_3, 140 nm of DLI ATI Al_2O_3 prepared at 420 °C, and 180 nm of DLI DMAI Al_2O_3 prepared at 500 °C. The z scale ranges from 0 to 50 nm. The roughness parameters derived from the measurements are listed in Table 2.

grown directly onto Si substrate (SI Fig. S2c and S2d). The morphology of alumina films prepared by DLI ATI differs significantly from that of the aforementioned films. The DLI ATI leads to the formation of agglomerated nodules along columns at 420 °C (Fig. 2c), which is similar to the morphology of the alumina films directly grown onto Si at 485 °C (SI Fig. S2a) and of that of a thicker Ti/Al_2O_3 bilayer stack prepared at 420 °C (SI Fig. S2b). Moreover, this difference in morphology is correlated to a significant difference in composition with the formation of a stoichiometric oxide using DLI DMAI at 500 °C [29], in contrast to the formation of partly hydroxylated aluminum oxide (O/Al = 1.80) when using DLI ATI at 420 °C [30].

The crystal structure of the Ti films before and after deposition of alumina was monitored using XRD. The starting films are nanocrystalline (SI Fig. S3a) and adopt the hexagonal α-Ti structure (P63/mmc space group). As is often observed during the growth of thin films, the films show texture and, as the thickness increases the preferential

Table 2 Roughness parameters derived from AFM measurements for 100 nm thick Ti films covered by 30 nm and 70 nm of ALD Al_2O_3, 140 nm of DLI ATI Al_2O_3 prepared at 420 °C, and 180 nm of DLI DMAI Al_2O_3 prepared at 500 °C, corresponding to Fig. 1. Values obtained for the alumina and Ti films deposited directly onto Si (SI Fig. S1) are given as references. S_a and S_q stand for the areal arithmetic and root mean squared roughness of an entire area scan, respectively. Values are in nm.

sample	S_a	S_q
Si/Al_2O_3 ALD 70 nm	0.23	0.34
Si/Al_2O_3 CVD ATI 140 nm	1.94	2.44
Si/Al_2O_3 CVD DMAI 180 nm	0.63	0.79
Si/Ti	5.11	6.31
$Si/Ti/Al_2O_3$ ALD 30 nm	3.94	5.03
$Si/Ti/Al_2O_3$ ALD 70 nm	2.99	3.83
$Si/Ti/Al_2O_3$ CVD ATI 140 nm	4.52	5.71
$Si/Ti/Al_2O_3$ CVD DMAI 180 nm	4.41	5.53

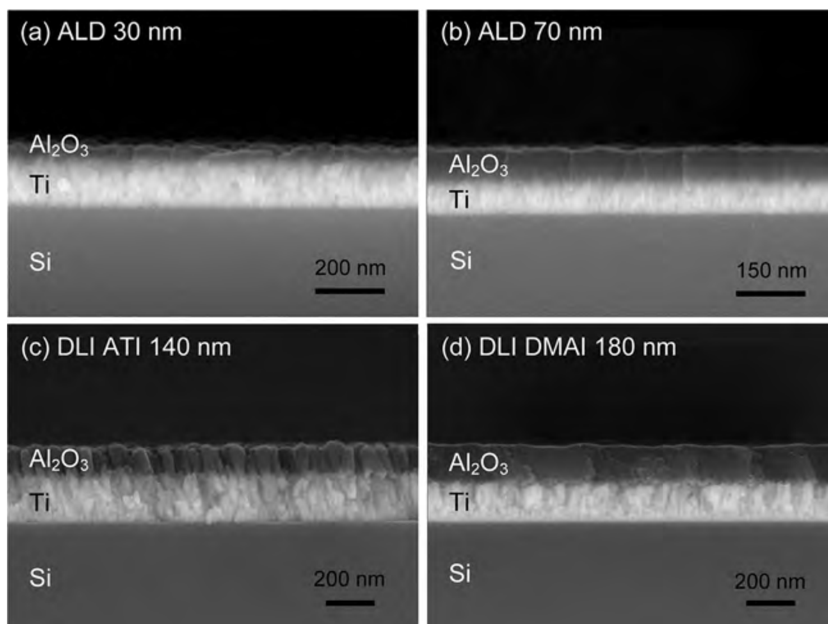

Figure 2 SEM cross-section micrographs of Ti films covered by (a) 30 nm of ALD Al_2O_3, (b) 70 nm of ALD Al_2O_3, (c) 140 nm of DLI ATI Al_2O_3 prepared at 420 °C, and (d) 180 nm of DLI DMAI Al_2O_3 prepared at 500 °C. Images were taken in backscattered mode. Note the different magnifications.

orientation of the nanocrystallites changes toward a texture closer to that expected for the randomly oriented reference pattern. After the DLI ATI at 485 °C, the crystal structure of the Ti film remained unchanged but a displacement of the diffraction peaks to lower angles was observed matching that of $TiO_{0.48}$ phase (SI Fig. S3b). The shift implies an increase of the lattice parameters (SI Table S1), as expected during the formation of $TiO_{0.5-x}$ hexagonal (P63/mmc) phase [31, 32].

In order to understand if these changes result from oxidation during the growth process of alumina or from pre-oxidation during the temperature ramp under vacuum with oxygen traces, a sample was annealed inside the CVD reactor at 2 Torr N_2 pressure at 485 °C without the addition of alumina precursor. The resulting diffraction pattern (SI Fig. S3b) shows the presence of $TiO_{0.325}$ phase, which adopts the same space group as α-Ti and $TiO_{0.48}$. Hence, this result either suggests that oxidation of the Ti film took place under vacuum with residual oxygen traces or that O impurities present in the starting sputtered Ti incorporated the α-Ti structure during post-annealing. The latter hypothesis was confirmed by the XPS results, as discussed later, and implies the sputter growth of Ti films with a residual amount of O not inserted in the α-Ti structure. The absence of O inserted in the α-Ti structure is supported by the lattice parameters matching those expected for pure Ti (SI Fig. S4 and Table S1). The presence of O may result from O stored in the grain boundaries of the polycrystalline target material, as observed with Cu targets for instance [33], and/or from trace impurities in the Ar gas (99.9995%). Moreover, Ti is a known O getter for ultra-high vacuum applications and is often employed in so-called "titanium sublimation pumps." It is thereby plausible that despite the low base pressure of the sputtering system (5×10^{-7} Torr), some of the O comes from residual contaminants of the sputter chamber.

During the introduction in the CVD reactor and pre-annealing to reach the steady-state deposition temperature, there is enough thermal energy for the Ti structure and O at the grains surface to intermix and form $TiO_{0.325}$. As the subsequent deposition of alumina takes places, further O coming from the CVD precursor can be incorporated into the Ti film, depending on the deposition duration and temperature, to lead to a composition up to $TiO_{0.48}$. The refined lattice parameters for the patterns shown in Fig. S3b are listed in Table S1 (SI), and comparison with crystallographic data from the PDF database is shown in SI Fig. S4. A good agreement is found and confirms the incorporation of O in the starting Ti structure in the form of TiO_x, with x up to ~0.5 [31, 32].

XPS depth profiling data for the starting Ti films, Ti films annealed at 485 °C in flowing N_2, and of Ti films oxidized in air at 600 °C to form pure rutile TiO_2 are shown in Fig. 3. In all cases, the surface of the films is fully oxidized into TiO_2, as evidenced by a binding energy around 458.5 eV in Ti $2p_{3/2}$ spectra. For the starting Ti films, as discussed above, the bulk of the film contains about 30 at.% O (Fig. 3a). Interestingly, this amount does not increase after annealing in the CVD reactor at 485 °C in flowing N_2, which highlights that the base pressure of the CVD reactor is low enough to prevent further oxidation of bulk Ti. In the case of TiO_2 (Fig. 3b), the composition remains almost constant from the surface to the bulk, which is in agreement with the full oxidation of Ti. However, it is clear from the Ti 2p high-resolution spectra that ion erosion rapidly and importantly reduces part of the Ti^{4+} ions to lower oxidation states. This change in oxidation state results from primary Ar ion bombardment, which can cause preferential sputtering,

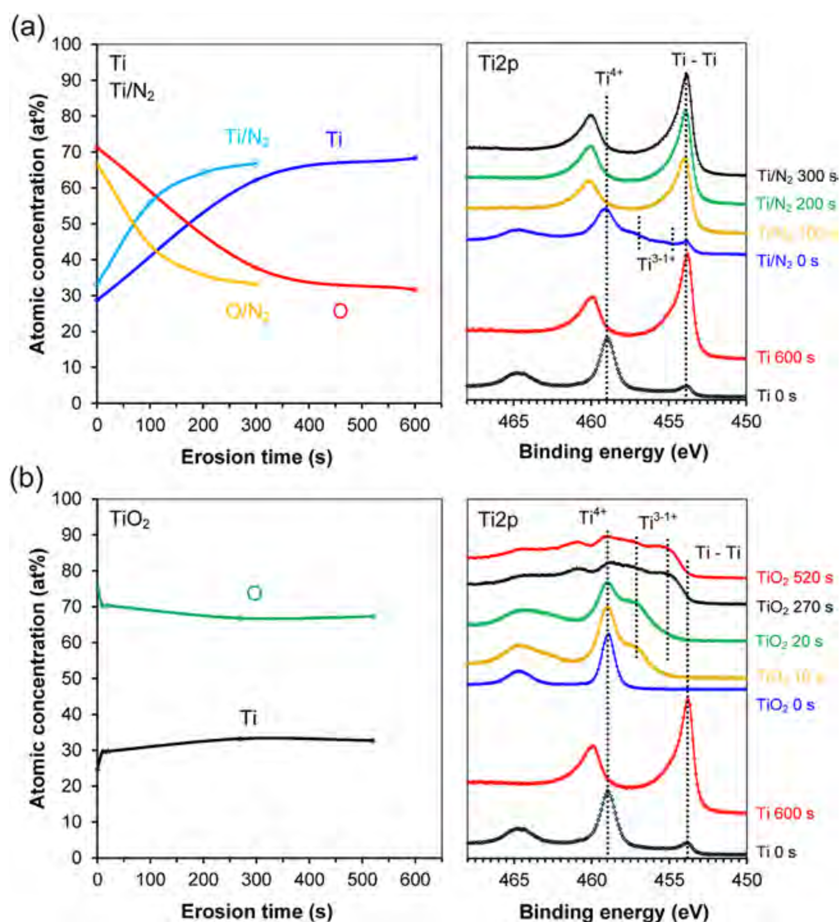

Figure 3 Depth profiles results for (a) Ti and Ti annealed at 485 °C in N_2, and for (b) TiO_2 thin film systems. The concentration profiles (left) and the Ti 2p X-ray photoelectron spectra (right) at various stages of erosion are presented.

important structural damage, and provokes the partial reduction of Ti^{4+} [34]. Although this effect limits the quantitative interpretation of the actual Ti oxidation state in the bulk of the film, qualitative information of the Ti/Al_2O_3 samples can be obtained by comparing the changes in Ti 2p signals for the various bilayer structures.

The XRD patterns of the Ti/Al_2O_3 bilayer stacks before and after post-annealing in air at 500 and 600 °C are shown in Fig. 4; they provide information on the impact of annealing conditions on the reactivity between the two phases. In order to minimize the extent of oxidation during alumina growth, the temperature during the DLI ATI was decreased to 420 °C, which prevents the oxidation into $TiO_{0.48}$ and yields the formation of $TiO_{0.325}$ (Fig. 4a). Moreover, for both ALD film thicknesses, the patterns match that of pure Ti (Fig. 4b). This result indicates the intermixing between α-Ti nanocrystallites and O stored at their boundaries does not take place at the lower temperature of 300 °C used in the ALD process. In contrast, this reaction takes place at 420 °C to form $TiO_{0.325}$, and further reaction occurs at 485 °C during the DLI ATI. Similarly, the Ti film is oxidized to a larger extent after the DLI DMAI at 500 °C, with the formation of $TiO_{0.48}$ (Fig. 4b). For this process, the rather slow growth rate practically prevents the use of deposition temperatures lower than 500 °C [29]. Moreover, the process with DMAI uses O_2 to compensate for the lower than 1.5 O/Al ratio in DMAI compared to ATI.

After post-annealing of the films obtained by DLI ATI, full oxidation into rutile TiO_2 is observed independently of the post-annealing temperature of 500 and 600 °C (Fig. 4a). This suggests poor oxygen barrier properties of this alumina material, which can originate from the porous morphology (Fig. 2 and SI Fig. S2) and the presence of hydroxyl groups as revealed by the off-stoichiometric composition (O/Al = 1.80) of the DLI ATI films [30]. For the alumina films prepared from the DLI DMAI and ALD processes, $TiO_{0.48}$ and Ti phases from the starting bilayer stack evolve after post-annealing at 500 °C for 65 h to a mixture of cubic Fm-3m TiO and hexagonal P63/mcm Ti_5Si_3 (Fig. 4c). It is worth recalling that cubic TiO is widely non-stoichiometric over the range of composition $0.8 \leq O/Ti \leq 1.2$ [31, 35–37]. The XRD patterns of the bilayer stacks of alumina films prepared by ALD and DLI DMAI that were post-annealed at 600 °C (Fig. 4d) show the presence of rutile TiO_2 along with the silicide Ti_5Si_3. These results support the backside reaction with Si and front side reaction with O. The O likely originates from diffusion of O from the air through the alumina film at high temperatures. Oxidation takes place even though the CVD alumina films are significantly thicker (140–180 nm) than the ALD films (30–70 nm). This

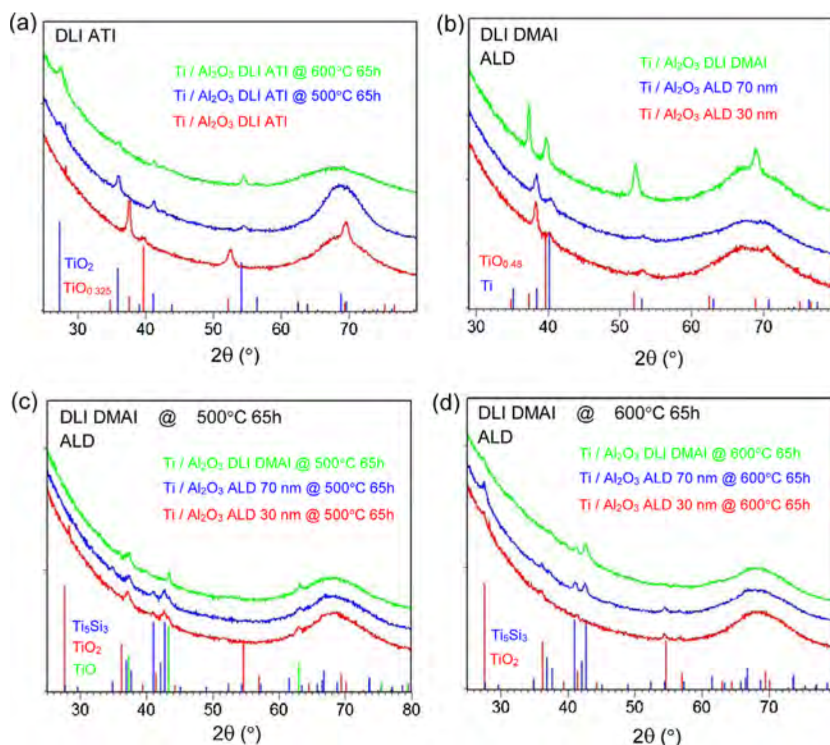

Figure 4 X-ray diffraction patterns of Si/Ti samples covered by (a) ~150 nm Al_2O_3 DLI ATI before and after thermal treatment at 500 and 600 °C in air for 65 h, (b) 30 and 70 nm Al_2O_3 ALD, and ~170 nm Al_2O_3 DLI DMAI. The patterns for the samples shown in (b) annealed at 500 and 600 °C for 65 h are presented in (c) and (d), respectively. Reference patterns hexagonal Ti, $TiO_{0.325}$, and $TiO_{0.48}$, cubic TiO, rutile TiO_2, and hexagonal Ti_5Si_3 phases are included when applicable.

suggests that at the higher temperatures, enough time is given for the diffusion of O.

The distribution, size, and identification of phases formed after annealing at 600 °C were further investigated by means of TEM on the Ti/Al_2O_3 stack prepared with 70 nm of ALD alumina (Fig. 5). The micrographs clearly show two distinct layers present on top of the Si substrate. The two layers consist of a crystalline film covered by an amorphous layer. The EDX line scan shows the presence of a layer rich in Ti and Si along with a small amount of O, which can suggest the formation of a Ti–Si alloy and TiO_2 clusters in the Ti film. The reaction between Si and Ti is well evidenced with the formation of large nanocrystals (see black arrows) expanding into the Si substrate. SAED and FFT patterns (Fig. 6) further confirm the formation of Ti_5Si_3 phase in the layer, in excellent agreement with the XRD data (Fig. 4). This result highlights the inhibition of O diffusion by the alumina film preventing the formation of oxide materials, in turn promoting the intermixing reaction between Si and Ti. The outer layer of the stack (Fig. 5) is mostly composed of Al and O elements along with a small amount of Ti. It is interesting to note that the alumina film remains amorphous, similar to the result obtained for a DLI DMAI film annealed in air at 500 °C (SI Fig. S5). Moreover, it is clear that the amorphous alumina layer has many inclusions of small crystallites up to the surface, which are most likely TiO_2 nanoparticles. This result highlights that it is important to consider the intermixing of Ti and Al_2O_3 as a possible root cause for O diffusion within alumina since Ti and TiO_2 are superior O conductor than Al_2O_3.

In order to further understand the intermixing of the materials, XPS depth profiling was conducted on the bilayer stacks before and after post-annealing in air. First, we will discuss the results for the ALD films of 30 nm (SI Fig. S6) and 70 nm (Fig. 7). The XPS results for the as-prepared (SI Figs. S6a and 7a) and 500 °C annealed (SI Figs. S6b and 7b) samples show the presence of the alumina film on the surface of partially oxidized Ti up to a O:Ti ratio of about 1:1, in good agreement with the XRD data. As the temperature increases to 600 °C (Figs. S6c and 7c), there seems to be a substantial increase in the amount of O stored in Ti up to the composition of TiO_2. For the 70 nm thick ALD film, an important decrease of the O content is observed at larger erosion depth. In both cases, there is little intermixing of Ti and Al_2O_3 films at 500 °C but significantly more intermixing occurs at 600 °C. Indeed, Ti is now present within the alumina film up to the surface, which is in very good agreement with the TEM data (Fig. 5) that evidenced the inclusion of Ti-containing nanoclusters up to the surface of alumina. Ti on the surface is fully oxidized into TiO_2, as shown by the binding energy around 458.5 eV in the Ti $2p_{3/2}$ spectra (SI Figs. S6c and 7c, right side). In the case of the 30 nm thick alumina film annealed at 600 °C, oxidation of Ti appears to take place over the entire measured thickness whereas the oxidation of the deeper part of the Ti film is partly prevented for the 70 nm thick ALD film. The latter result is visible in the Ti 2p spectra showing signals of Ar-ion-reduced TiO_2 for the 30 nm thick film (Fig. S6c and Fig. 3b) whereas signals attributed to TiO_x ($x < 1$) and Ti^0 (Ti metal or Ti–Si) are measured around 454 eV in Ti $2p_{3/2}$ at high erosion depths

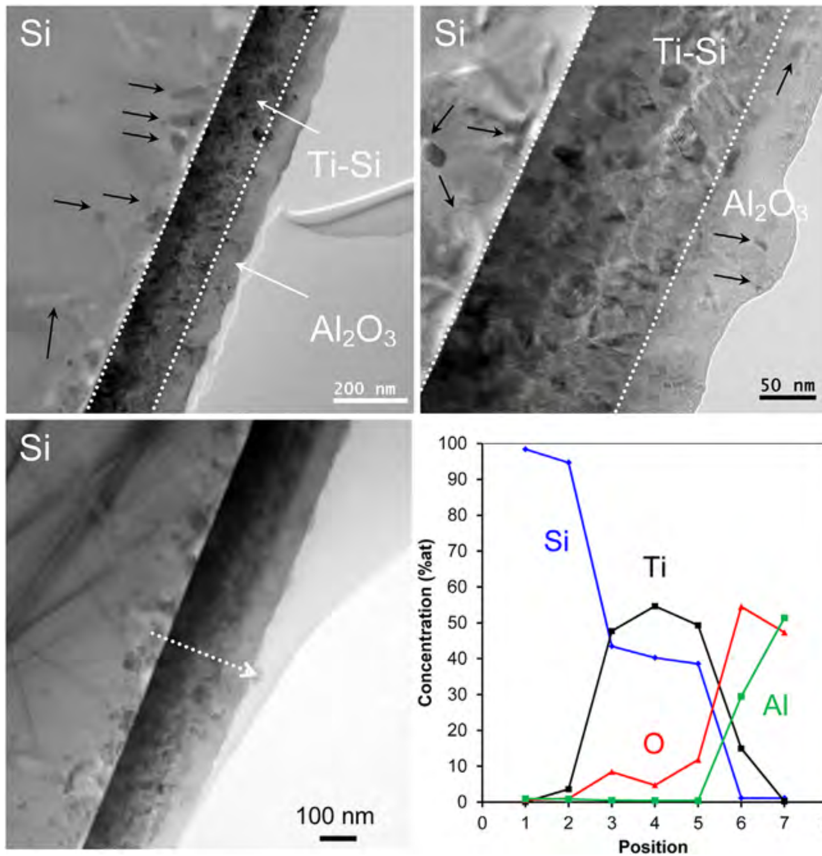

Figure 5 TEM micrographs of the bilayer stack consisting of a Ti layer covered by a 70 nm thick ALD alumina film post-annealed at 600 °C. The white arrows indicate the Ti–Si and Al_2O_3 layers and the black arrows highlight some of the products formed between Si and Ti, and Ti and Al_2O_3 materials. The concentrations obtained by EDX across the Si/Ti/Al_2O_3 stack (dashed arrow) are shown in the lower graph.

for the 70 nm thick film (Figs.7c and 3b). This result complements the results obtained with XRD and TEM that showed the formation of Ti_5Si_3 at the Si/Ti interface where Ti is expected to display a metallic character in this phase. In summary, these results demonstrate that thin ALD films (30–70 nm) can prevent the full oxidation of Ti when annealing at 500 °C is conducted for 65 h, however, they do not prevent O diffusion and the partial oxidation of Ti. Moreover, further oxidation of Ti can partially take place at higher temperatures (600 °C and above). Finally, it is striking to observe a significant efficiency in the oxidation barrier properties when a thin 70 nm alumina film is used,

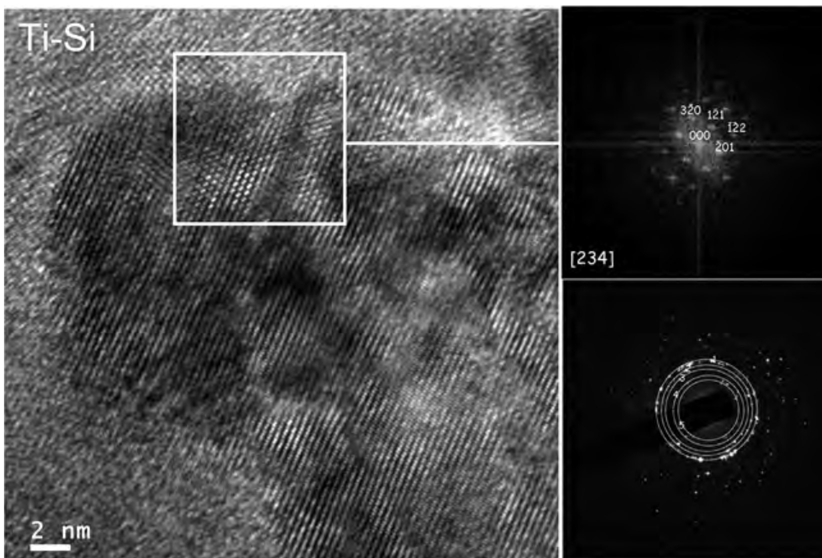

Figure 6 HRTEM micrographs, FFT pattern of a crystallite fringes (upper right), and SAED pattern (lower right) of the Ti layer covered by an ALD 70 nm thick alumina film post-annealed at 600 °C (Fig. 5). Indexing of the diffraction spots (SI Table S2) confirms the presence of P63/mcm Ti_5Si_3 phase.

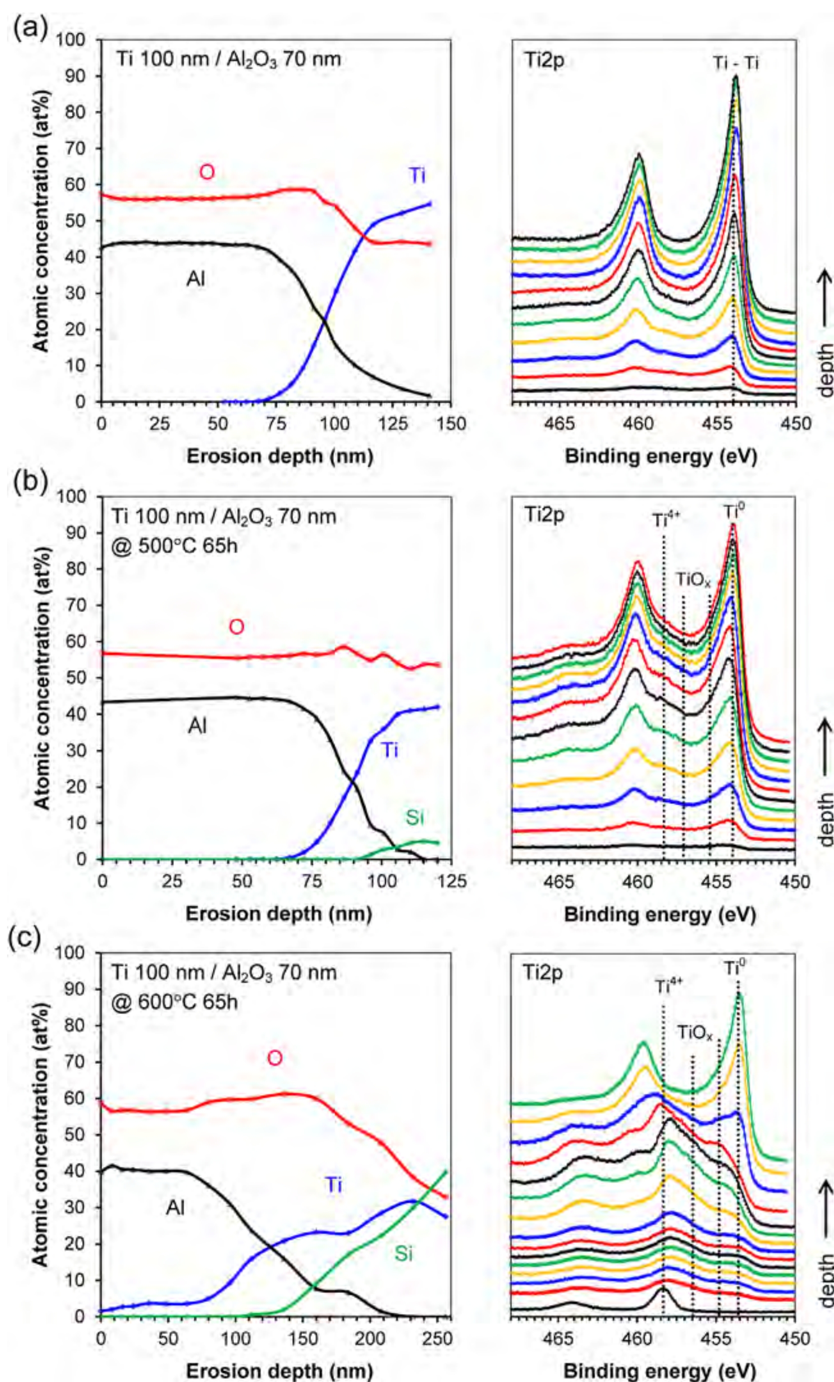

Figure 7 Depth profiles results for (a) an as-prepared Ti/Al_2O_3 70 nm (ALD) bilayer stack, and Ti/Al_2O_3 70 nm (ALD) bilayer stacks annealed in air 65 h at (b) 500 °C and (c) 600 °C. The concentration profile (left) and Ti 2p X-ray photoelectron spectra at various stages of erosion (right) are presented.

as evidenced by the absence of full oxidation of the inner part of the Ti layer.

In contrast, when Ti is covered by a 150 nm thick alumina film produced by the DLI ATI (SI Fig. S7), annealing at 500 or 600 °C leads in both cases to the oxidation of Ti into TiO_2, as already observed with XRD (Fig. 4a). This result further supports the poor oxidation barrier properties of this type of alumina material. Indeed, the composition of the films obtained by DLI ATI deviates from stoichiometry [30], and the films are composed of agglomerated nodules in the form of columns with apparent internal porosity (Fig. 2c and SI Fig. S2a and S2b) [29], which may more easily allow O diffusion toward the Ti film. In summary, these results illustrate that the thickness of the alumina film is not a crucial requirement for an oxidation barrier but instead the morphology, stoichiometry and local coordination order are critical factors to the good properties [28].

Alumina films obtained by the DLI DMAI at 500 °C in the presence of O_2 are good candidates as oxygen barriers as the films are stoichiometric, and show a compact structure

(Fig. 2d and SI Fig. S2c) [29]. After annealing in air, films of about 180 nm show a behavior similar to the ALD films with the partial oxidation of Ti at 500 °C (Fig. 8b) and a more profound oxidation at 600 °C (Fig. 8c). In the case of these films, the intermixing of Ti with Al_2O_3 is much lower than for the ALD films with fairly narrow diffusion zones (Fig. 8b and c). Moreover, there is no evidence for the presence of Ti near the outer alumina surface or included in the alumina film far from the interface. This contrasts with the results of the ALD films for which Ti was measured about 70 nm apart from the initial Ti/Al_2O_3 interface, and indicates the beneficial role of the DLI DMAI films for preventing intermixing with Ti. The reasons for the improvement cannot solely be related to the larger film thickness as no Ti was detected by XPS at 50–100 nm from the initial Ti/Al_2O_3 interface (Fig. 8c), and suggests that the film density and local atomic structure can prevent Ti and Al_2O_3 interdiffusion. Further work is necessary to elucidate the differences in local atomic structure of these DLI DMAI and ALD alumina films.

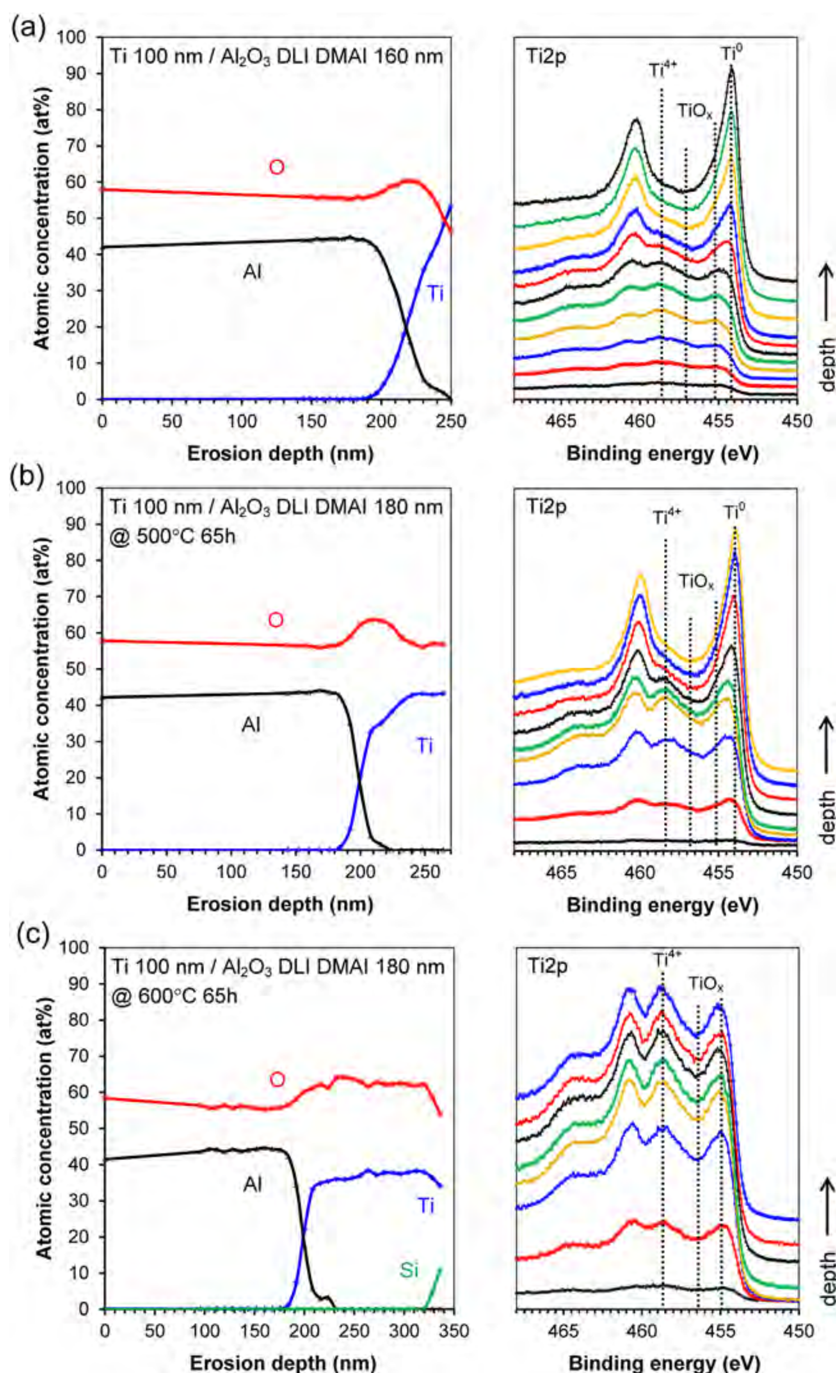

Figure 8 Depth profiles results for (a) an as-prepared Ti/Al_2O_3 (DLI DMAI) bilayer stack, and Ti/Al_2O_3 (DLI DMAI) bilayer stacks annealed in air 65 h at (b) 500 °C and (c) 600 °C. The concentration profile (left) and Ti 2p X-ray photoelectron spectra at various stages of erosion (right) are presented.

4 Conclusions Ti/Al_2O_3 bilayer stacks were used as model systems for the investigation of Ti protection from medium temperature (500–600 °C) oxidation by using amorphous alumina thin films of 30–180 nm thickness as oxygen barriers. The films produced from the DLI ATI are very poor oxygen barriers. In opposition, the films processed using the ALD of TMA show good barrier properties but an extensive intermixing with Ti is monitored, followed by the subsequent oxidation of Ti. With a stark contrast, the films prepared from DLI DMAI offer excellent oxygen barrier properties and show little intermixing with Ti. In summary, these measurements correlate the effect of the alumina coating thickness, morphology, and stoichiometry resulting from the preparation method to the oxidation barrier properties, and show that compact and stoichiometric amorphous alumina films offer superior barrier properties.

Supporting Information

Additional supporting information may be found in the online version of this article at the publisher's web-site.

Acknowledgements This work was financially supported by the STAE-RTRA foundation (Toulouse, France) under the RTRA-STAE/2014/P/VIMA/12 project grant. The U.S. Department of Energy (DOE), Basic Energy Sciences (BES), Materials Sciences and Engineering Division supported a portion of this work (G.M.V., Ti thin film preparation).

References

[1] H. Klauk, Nature Mater. **8**, 853 (2009).
[2] M. Trueba and S. P. Trasatti, Eur. J. Inorg. Chem. **17**, 3393 (2005).
[3] S. Blittersdorf, N. Bahlawane, K. Kohse-Höinghaus, B. Atakan, and J. Müller, Chem. Vap. Deposition **9**, 194 (2003).
[4] S. S. Yom, W. N. Kang, Y. S. Yoon, J. I. Lee, D. J. Choi, T. W. Kim, K. Y. Seo, P. H. Hur, and C. Y. Kim, Thin Solid Films **213**, 72 (1992).
[5] G. M. Veith, A. R. Lupini, S. J. Pennycook, G. W. Ownby, and N. J. Dudney, J. Catalysis **231**, 151 (2005).
[6] I. Levin and D. Brandon, J. Am. Ceram. Soc. **81**, 1995 (1998).
[7] H.-M. Cheng, F.-M. Wang, J. P. Chu, R. Santhanam, J. Rick, and S.-C. Lo, J. Phys. Chem. C **116**, 7629 (2012).
[8] Y. He, X. Yu, Y. Wang, H. Li, and X. Huang, Adv. Mater. **23**, 4938 (2011).
[9] L. Baggetto, N. J. Dudney, and G. M. Veith, Electrochim. Acta **90**, 135 (2013).
[10] M. Vasilopoulou, D. G. Georgiadou, A. Soultati, N. Boukos, S. Gardelis, L. C. Palilis, M. Fakis, G. Skoulatakis, S. Kennou, M. Botzakaki, S. Georga, C. A. Krontiras, F. Auras, D. Fattakhov-Rohlfing, T. Bein, T. A. Papadopoulos, D. Davazoglou, and P. Argitis, Adv. Energy Mater. **4**, 1400214 (2014).
[11] A.-M. Lazar, W. P. Yespica, S. Marcelin, N. Pébère, D. Samélor, C. Tendero, and C. Vahlas, Corros. Sci. **81**, 125 (2014).
[12] S. Krumdieck, S. Davies, C. M. Bishop, T. Kemmitt, and J. V. Kennedy, Surf. Coat. Technol. **230**, 208 (2013).
[13] J. H. Perepezko, Science **326**, 1068 (2009).
[14] A. G. Evans, D. R. Clarke, and C. G. Levi, J. European Ceram. Soc. **28**, 1405 (2008).
[15] J. P. Rivière, L. Pichon, M. Drouet, A. Galdikas, and D. Poquillon, Surf. Coat. Technol. **200**, 5498 (2006).
[16] A. M. Kliauga and M. Ferrante, J. Mater. Sci. **35**, 4243 (2000).
[17] S. Kang and J. H. Selverian, J. Mater. Sci. **27**, 4536 (1992).
[18] H. J. Kang, C. H. Kim, J. H. Kim, and C. N. Whang, J. Korean Phys. Soc. **31**, 158 (1997).
[19] O. M. Ndwandwe and M. S. Mpungose, S. Afr. J. Sci. **102**, 244 (2006).
[20] P. R. von Rohr and B. Borer, Chem. Vap. Deposition **13**, 499 (2007).
[21] H. C. M. Knoops, M. E. Donders, M. C. M. van de Sanden, P. H. L. Notten, and W. M. M. Kessels, J. Vac. Sci. Technol. A **30**, 010801 (2012).
[22] F. Vanni, B. Caussat, C. Ablitzer, X. Iltis, and M. Bothier, Phys. Status Solidi A **212**, 1599 (2015).
[23] L. Baggetto, H. C. M. Knoops, R. A. H. Niessen, W. M. M. Kessels, and P. H. L. Notten, J. Mater. Chem. **20**, 3703 (2010).
[24] F. Roozeboom, A. L. A. M. Kemmeren, J. F. C. Verhoeven, F. C. van den Heuvel, J. Klootwijk, H. Kretschman, T. Fric, E. C. E. van Grunsven, S. Bardy, C. Bunel, D. Chevrie, F. LeCornec, S. Ledain, F. Murray, and P. Philippe, Thin Solid Films **504**, 391 (2006).
[25] R. Gordon, J. Non-Cryst. Solids **218**, 81 (1997).
[26] A. N. Gleizes, C. Vahlas, M.-M. Sovar, D. Samélor, and M.-C. Lafont, Chem. Vap. Deposition **13**, 23 (2007).
[27] Y. Balcaen, N. Radutoiu, J. Alexis, J.-D. Beguin, L. Lacroix, D. Samélor, and C. Vahlas, Surf. Coat. Technol. **206**, 1684 (2011).
[28] V. Sarou-Kanian, A. N. Gleizes, P. Florian, D. Samélor, D. Massiot, and C. Vahlas, J. Phys. Chem. C **117**, 21965 (2013).
[29] L. Baggetto, J. Esvan, C. Charvillat, D. Samélor, H. Vergnes, B. Caussat, A. Gleizes, and C. Vahlas, Phys. Status Solidi C **12**, 989 (2015).
[30] P.-L. Etchepare, L. Baggetto, H. Vergnes, D. Samélor, D. Sadowski, B. Caussat, and C. Vahlas, Phys. Status Solidi C **12**, 944 (2015).
[31] S. Andersson, B. Collén, U. Kuylenstierna, and A. Magnéli, Acta Chem. Scand. **11**, 1641 (1957).
[32] B. Holmberg, Acta Chem. Scand. **16**, 1245 (1962).
[33] S. Lee, J. Y. Kim, T.-W. Lee, W.-K. Kim, B.-S. Kim, J. H. Park, J.-S. Bae, Y. C. Cho, J. Kim, M.-W. Oh, C. S. Hwang, and S.-Y. Jeong, Sci. Rep. **4**, 6230 (2014).
[34] J. D. P. Counsell, A. J. Roberts, W. Boxford, C. Moffitt, and K. Takahashi, J. Surf. Anal. **20**, 211 (2014).
[35] M. E. Straumanis and H. W. Li, Anorg. Allg. Chem. **305**, 143 (1969).
[36] V. Dufek, F. Petru, and V. Brozek, Monatsh. Chem. **98**, 2424 (1967).
[37] R. E. Loehman, C. N. R. Rao, and J. M. Honig, J. Phys. Chem. **73**, 1781 (1969).